A Super-Twisting Observer Design for Thrust-Loss Fault Tolerant Control of Quadrotor Vehicles

D. M. K. K. Venkateswara Rao[1], Hamed Habibi[1], Prathyush P. Menon[2], Christopher Edwards[3], and Holger Voos[1,4]

***Abstract*— In this paper, we tackle the thrust loss problem in a quadrotor unmanned aerial vehicle, by the design of a super-twisting observer in the body frame, achieving finite-time convergence. On this basis, we design a super-twisting low-level controller to track the desired trajectory and compensate for the loss effects. Then, the acceleration commands are designed, and the thrust, Euler angles, and angular speeds are computed. The stability and the finite-time convergence of the resultant cascade system are studied, and we show the recovery of the nominal behavior, as well as the weak recovery of the separation principle. Finally, high-fidelity experimental analyses are conducted, to evaluate the performance of the proposed algorithm in the presence of a variety of thrust loss situations.**

SUPPLEMENTARY MATERIAL

Video: https://youtu.be/IPZ4OvBH85U

I. INTRODUCTION

Safe and reliable operation of quadrotor Unmanned Aerial Vehicles (UAVs) has been a subject of significant attention in the past decade [1]. This interest is increasing as a result of increasingly stringent regulations, addressing problems such as UAV recovery during a malfunction, or safety certification without complex hardware [2]. Moreover, the operators favor more autonomous navigation, which signifies the importance of safety and reliability. However, the need for fast and accurate tracking performance, uncertainty robustness, and malfunctioning resilience cannot be satisfactorily achieved by existing onboard autopilots [3]. This can be addressed by incorporating separate safety and reliability measures that complement the autopilot's low-level control algorithm [1].

UAVs are prone to deterioration of performance and safety, as a result of issues such as blade deformation, cracks, debris built-up, motor/software failure, low battery levels, or battery malfunction, and oscillation of propeller guards [3, 4]. This can translate into a thrust-loss type of fault, which, in turn, downgrades the tracking performance, and leads to safety violations [5]. Therefore, Fault Tolerant Control (FTC) approaches have been considered for UAV control design to retain reliability and safety at the desired level [6]. Although passive FTC approaches can be employed by designing a robust controller for the worst-case scenario, with associated conservativeness, active FTC is a more attractive paradigm, with the design of an estimator serving as software redundancy. This estimation is then used for the control modification and monitoring [7].

For high tracking performance of UAVs, it is required to design the controller at a low level, eliminating the reliance on the autopilot, which has poor performance at higher speeds [8–10]. Also, the Finite-Time (FT) convergence is important for UAVs, as a certificate of system safety [3]. This is because a small deviation from the desired orientation, or a fault might lead to a catastrophe [11, 12]. With FT convergence, one can guarantee the recovery of the nominal performance within a specific time window, which is imposed by the regulatory bodies [2, 13]. Furthermore, aerodynamic effects, such as lift and drag, should be carefully treated in the modeling, on which basis the estimator and the controller are designed. Otherwise, the estimator might mistake those effects for faults, or, the controller might command extra effort to handle them, which, in turn, leads to chattering [14, 15]. For tackling thrust loss, it is desirable to have the estimator designed in the body frame to have a better estimation [3]. Otherwise, the projected component of the loss is to be estimated in each direction in the inertial frame, which, combined, leads to inaccurate estimation [1, 16].

Motivated by these considerations, we design a Super-Twisting Observer (STO) to estimate the thrust loss, with FT convergence. Here, we design an STO in the UAV body frame. Then, we design a Super-Twisting Controller (STC), taking into account the estimated thrust loss. The low-level acceleration commands are so designed, on which basis we design the required thrust, desired Euler angles, and angular speeds, to track the desired trajectory and to compensate for the loss effect. The main contributions are as follows:

- We design the STO in the body frame with FT convergence in contrast to [1, 3, 14]. In [14] the estimation is highly dependent on the time constant of the low-pass filter. However, this is relaxed in this paper. The low-level STC is designed in the inertial frame, and we study the stability and convergence of the cascade system. Then, we show the recovery of the nominal behavior in the presence of the thrust loss. We further show the "weak" recovery of the separation principle, in contrast to some works, *e.g.*, [1,

[1]D.M.K.K. Venkateswara Rao (corresponding author), Hamed Habibi, and Holger Voos are with the Automation and Robotics Research Group, Interdisciplinary Centre for Security, Reliability and Trust, University of Luxembourg, Luxembourg. mohan.dasari@uni.lu, hamed.habibi@uni.lu, holger.voos@uni.lu

[2]P. Menon is with Cooperative Robotics and Autonomous NEtworks (CRANE) lab at the Centre for Future Clean Mobility, University of Exeter Engineering Research Centre, Exeter EX5 2GD, UK. P.M.Prathyush@exeter.ac.uk

[3]Christopher Edwards is with Structure and Dynamics Research Group, CEMPS, University of Exeter, Exeter, UK. C.Edwards@exeter.ac.uk

[4]Holger Voos is also with the Faculty of Science, Technology, and Medicine (FSTM), Department of Engineering, University of Luxembourg.

3, 14, 15, 17]. The low-level controller is designed, for agile maneuvering and accurate tracking, superceding some works, *e.g.*, [18–20].

• We experimentally identify the aerodynamic model of the UAV, on which basis high-fidelity experimental analyses are conducted which demonstrate accurate tracking performance. This highlights the applicability of the proposed method in practice, compared to some works, *e.g.*, [8–14], in which only numerical simulations are carried out. We also consider a variety of faults, both additive and effectiveness losses, with both abrupt and gradual occurrences.

In this paper underlined letters, *e.g.*, $\underline{x}$, and $\underline{x}^B$ represent a vector in the inertial and the body coordinates, respectively. $\mathbb{R}$ denotes the set of real numbers set. $\mathsf{SO(3)}$ represents special orthogonal matrices. $|x|$ and $||\underline{x}||$ denote the absolute value of the scalar and the Euclidean norm of the vector, respectively. $g = 9.81(m/s^2)$ represents gravity. Finally, $\times$ denotes the cross product of vectors.

II. MODEL DESCRIPTION AND PRELIMINARIES

The dynamics of a UAV can be presented as [21]

$$\dot{\underline{x}}(t) = \underline{v}(t), \tag{1a}$$

$$\dot{\underline{v}}(t) = \frac{1}{M}\left(R(t)\underline{F}^B_{th}(t) - \underline{L}(t) - \underline{D}(t) - M\underline{g} - R(t)\underline{F}^B_{loss}(t)\right), \tag{1b}$$

$$\dot{\underline{\Phi}}(t) = R_q^{-1}(t)\underline{\omega}^B(t), \tag{1c}$$

$$\dot{\underline{\omega}}^B(t) = J^{-1}\left(\underline{\tau}^B(t) - \underline{\omega}^B(t)\times J\underline{\omega}^B(t)\right), \tag{1d}$$

where, $\underline{x}(t) = [x(t), y(t), z(t)]^T \in \mathbb{R}^3$ and $\underline{v}(t) = [v_x(t), v_y(t), v_z(t)]^T \in \mathbb{R}^3$ are the center of mass' position and velocity vectors, respectively, $\underline{L}(t) = [0,0,L_z(t)]^T = C_L[0,0,\|\underline{v}(t)\|^2]^T \in \mathbb{R}^3$ and $\underline{D}(t) = [D_x(t), D_y(t), D_z(t)]^T = C_D\|\underline{v}(t)\|\underline{v}(t) \in \mathbb{R}^3$ are lift and drag vectors, respectively, all in the inertial frame, where C_L and C_D are the lift and drag coefficients, respectively. $\underline{\omega}^B(t) = [p(t), q(t), r(t)]^T \in \mathbb{R}^3$ is the angular velocity in the body frame. M is the mass and $J \in \mathbb{R}^{3\times 3}$ is the mass moment inertia. The quantities $\underline{\Phi}(t) = [\phi(t), \theta(t), \psi(t)]^T \in \mathbb{R}^3$ is the Euler angle vector and $\underline{F}^B_{th}(t) = [0,0,f_{th}(t)]^T \in \mathbb{R}^3$ is the thrust vector in the body frame. $\theta(t)$, $\phi(t)$ and $\psi(t)$ denote pitch, roll and yaw angles, respectively. $f_{th}(t) \in \mathbb{R}_+$ is thrust and $\underline{g} = [0,0,g]^T \in \mathbb{R}^3$ is the vector of gravity in the inertial frame whilst $\underline{\tau}^B(t) \in \mathbb{R}^3$ is the torque vector in the body frame. $\underline{F}^B_{loss}(t) = [0,0,f_{loss}(t)]^T \in \mathbb{R}^3$ is the thrust loss vector, where $f_{loss}(t)$ is the actual thrust loss. The rotation matrix $R(t) \in \mathsf{SO(3)}$ from body to inertial frame, and the transformation matrix $R_q(t) \in \mathsf{SO(3)}$ are as [22]:

$$R(t) = \begin{bmatrix} C_\psi C_\theta & C_\psi S_\theta S_\phi - S_\psi C_\phi & C_\psi S_\theta C_\phi + S_\psi S_\phi \\ S_\psi C_\theta & S_\psi S_\theta S_\phi + C_\psi C_\phi & S_\psi S_\theta C_\phi - C_\psi S_\phi \\ -S_\theta & C_\theta S_\phi & C_\theta C_\phi \end{bmatrix}, \tag{2a}$$

$$R_q(t) = \begin{bmatrix} 1 & 0 & -S_\theta \\ 0 & C_\phi & C_\theta S_\phi \\ 0 & -S_\phi & C_\theta C_\phi \end{bmatrix}, \tag{2b}$$

where, C_α and S_α denote cosine and sine of $\alpha(t)$, respectively. $\underline{v}^B(t) = R^{-1}(t)\underline{v}(t) = [v^B_x(t), v^B_y(t), v^B_z(t)]^T \in \mathbb{R}^3$, $\underline{D}^B(t) = R^{-1}(t)\underline{D}(t) = [D^B_x(t), D^B_y(t), D^B_z(t)]^T \in \mathbb{R}^3$, $\underline{L}^B(t) = R^{-1}(t)\underline{L}(t) = [L^B_x(t), L^B_y(t), L^B_z(t)]^T \in \mathbb{R}^3$ are the velocity, drag, and lift vectors in the body frame. It is easy to obtain

$$\begin{aligned}\dot{\underline{v}}^B(t) =& -\underline{\omega}^B(t)\times\underline{v}^B - \frac{1}{M}R^{-1}(t)(\underline{D}(t) + \underline{L}(t) + M\underline{g}) \\ &+ \frac{1}{M}\left(\underline{F}^B_{th}(t) - \underline{F}^B_{loss}(t)\right),\end{aligned} \tag{3}$$

which in the z-axis yields

$$\begin{aligned}\dot{v}^B_z(t) =& q(t)v^B_x(t) - p(t)v^B_y(t) - \frac{1}{M}(D^B_z(t) + L^B_z(t)) \\ &- C_\theta C_\phi g + \frac{1}{M}\left(f_{th}(t) - f_{loss}(t)\right).\end{aligned} \tag{4}$$

The term $f_{loss}(t)$ appears in the z axis of the body frame and it is more accurate to estimate it there than in the inertial frame where a portion of it appears in each direction. Considering (4), we design an STO to estimate the thrust loss $f_{loss}(t)$. The estimated signal $\hat{f}_{loss}(t)$ is then used to compensate the loss effect and, accordingly, we design the desired thrust $f_{th}(t)$, desired Euler angle $\underline{\Phi}_d(t) = [\phi_d(t), \theta_d(t), \psi_d(t)]^T \in \mathbb{R}^3$ and desired angular velocity $\underline{\omega}_d(t)$, using (1), to steer the UAV position $\underline{x}(t)$ towards the desired trajectory $\underline{x}_d(t) = [x_d(t), y_d(t), z_d(t)]^T \in \mathbb{R}^3$, for any initial conditions $\underline{x}(0)$.

Assumption 1. *It is assumed that $\underline{x}$, $\underline{v}$, $\underline{v}^B$, $\underline{\Phi}$ and $\underline{\omega}^B$ are all available [14]. The desired trajectory $\underline{x}_d(t)$ is known and continuous up to the second time derivative [4]. Furthermore, it is assumed that the fault is bounded and $|f_{loss}| \le \bar{f}_0$ and its time derivative is bounded as $|\dot{f}_{loss}(t)| \le \bar{f}_1$ [6]. In (1b), it is assumed that the total thrust loss is uniformly distributed across all the motors [7]. The aerodynamic model in (1b) is from [13] and the coefficients C_L and C_D are assumed to be constant and obtained experimentally.*

Lemma 1. *[23, 24] Consider the super-twisting dynamics*

$$\dot{X}_1(t) = -k_1|X_1(t)|^{\frac{1}{2}}\,\mathrm{sign}\,(X_1(t)) + X_2(t), \tag{5a}$$

$$\dot{X}_2(t) = -k_2\,\mathrm{sign}\,(X_1(t)) + d. \tag{5b}$$

Assume $|d| \le d_1$ where d_1 is a positive constant. Then, by choosing $k_1 > 0$ and $k_2 > 0$ properly, the solution (5), i.e., $X(t) = [X_1(t), X_2(t)]^T$ converges to zero in FT, for any initial condition $X_0 = X(0)$, i.e., the origin is a robustly globally FT stable equilibrium point. This further yields convergence of $\dot{X}_1(t)$ to zero in FT, simultaneously. The solution of (5) needs to be understood in a Filippov sense.

Remark 1. *As an extensively adopted convention, suggested in [24], the gains of (5) can be selected as $k_1 = 1.5\sqrt{d_1}$ and $k_2 = 1.1d_1$, to achieve FT convergence for $X(t)$, i.e., solution of (5), satisfying the Algorithm 1 in [23].*

Lemma 2. *[25, Theorem 5.1] Consider the cascade system Π as follows.*

$$\Pi \triangleq \begin{cases} \dot{X}_1(t) = f_1(X_1) + f_2(X_2) \triangleq f(X_1, X_2) \\ \dot{X}_2(t) = g(X_2), \end{cases} \tag{6}$$

with state vector $X \triangleq [X_1, X_2]^T$. Let $X_2(t)$ converge to zero in FT, i.e., $X_2(t) = 0$ for $t \geq T(X_2(0))$. Also, assume $\dot{X}_1(t) = f_1(X_1) + d(t)$ converges to zero in FT for a bounded and vanishing disturbance $d(t)$. Also, $X_1(t)$ cannot escape to infinity in FT. Furthermore, $f_2(X_2)$ is bounded and vanishes, i.e., $\int_0^\infty f_2(X_2(\tau))d\tau$ is finite. Then, the origin of the cascade system Π is FT stable.

III. OBSERVER BASED CONTROLLER DESIGN

To estimate the thrust loss f_{loss} in the body frame, we use (4) and design an STO as

$$\begin{aligned}\dot{\hat{v}}(t) = q(t)v_x^B(t) - p(t)v_y^B(t) - \frac{1}{M}(D_z^B(t) + L_z^B(t)) \\ - C_\theta C_\phi g + \frac{1}{M}\left(f_{th}(t) - \hat{f}_{loss}(t)\right),\end{aligned} \tag{7}$$

where the fault estimation is given by

$$\hat{f}_{loss}(t) = \alpha |e_v(t)|^{\frac{1}{2}} \operatorname{sign}(e_v(t)) + \nu_1(t), \tag{8a}$$

$$\dot{\nu}_1(t) = \beta sign(e_v(t)), \tag{8b}$$

where $e_v(t) = M(\hat{v}(t) - v_z^B(t))$. The main properties of the observer (7) and (8) are discussed in the following lemma.

Lemma 3. *Consider the dynamics in the body frame as in (4). Design an observer as in (7) with the fault estimation as in (8). Let $\mu(t) \triangleq -\nu_1(t) + f_{loss}(t) = -\beta \int_0^t \operatorname{sign}(e_v(\tau))d\tau + f_{loss}(t)$. Then, setting $\alpha = 1.5\sqrt{\bar{f}_1}$ and $\beta = 1.1\bar{f}_1$ creates a second-order sliding mode in FT $T_o(e_v(0), \mu(0))$, i.e., both $e_v(t)$ and $\dot{e}_v(t)$ converge to zero $\forall t \geq T_o(\cdot)$. This further implies that the fault estimation error $e_f(t) = f_{loss}(t) - \hat{f}_{loss}(t)$ converges to zero in finite time. Also, for $0 \leq t \leq T_o(\cdot)$, $\mu(t)$ remains bounded and converges to zero at $T_o(\cdot)$.*

Proof: Using (7), (8), and (4), it is easy to show that

$$\Pi_{obs} \triangleq \begin{cases} \dot{e}_v(t) = -\alpha\, |e_v(t)|^{\frac{1}{2}} \operatorname{sign}(e_v(t)) + \mu(t) \\ \dot{\mu}(t) = -\beta \operatorname{sign}(e_v(t)) + \dot{f}_{\text{loss}}(t). \end{cases} \tag{9}$$

Considering Lemma 1 and Remark 1, by choosing $\alpha = 1.5\sqrt{\bar{f}_1}$ and $\beta = 1.1\bar{f}_1$ one can obtain that $e_v(t)$ and $\mu(t)$ converge to zero in FT, *i.e.*, $\forall t \geq T_o(e_v(0), \mu(0))$. Also, $\dot{e}_v(t)$ converges to zero in FT, simultaneously with $e_v(t)$. On the other hand, it is readily shown that $\dot{e}_v(t) = f_{loss}(t) - \hat{f}_{loss}(t)$. This further yields $\hat{f}_{loss}(t)$ converges to $f_{loss}(t)$ in FT. Since $e_v(t)$ and $\dot{e}_v(t)$ are bounded and go to zero, therefore, $\alpha|e_v(t)|^{\frac{1}{2}} \operatorname{sign}(e_v(t)) = 0$, at $t = T_o(\cdot)$. Consequently, one can obtain that $\mu(T_o(\cdot)) = 0$. Furthermore, $\int_0^{T_o} \operatorname{sign}(e_v(\tau))d\tau$ is bounded and $f_{loss} \leq \bar{f}_0$. So, $\mu(t)$ remains bounded for any initial condition $e_v(0)$, $\mu(0)$, $f_{loss}(0)$, and $0 \leq t \leq T_o(\cdot)$. □

Remark 2. *The STC is designed considering dynamics in the inertial frame, but as the fault happens only along the z axis in the body frame, only a one-dimensional observer needs to be designed using (4). Otherwise, a three-dimensional observer needs to be designed in the inertial frame to capture the transformed fault and renormalize it. This could be corrupted with other uncertainties, leading to high estimation errors. Also, it is more practical to assume an upper bound for the rate of evolution of fault as in Lemma 3, rather than the fault magnitude [6]. Furthermore, the observer gains in (7)-(8), can be easily made adaptive for unknown $\bar{f}_1$.*

Now, to design the control, we define sliding surfaces as

$$\sigma_x(t) = (v_x(t) - v_{d,x}(t)) + \lambda_x(x(t) - x_d(t)), \tag{10a}$$

$$\sigma_y(t) = (v_y(t) - v_{d,y}(t)) + \lambda_y(y(t) - y_d(t)), \tag{10b}$$

$$\sigma_z(t) = (v_z(t) - v_{d,z}(t)) + \lambda_z(z(t) - z_d(t)), \tag{10c}$$

where $\underline{v}_d(t) = [v_{d,x}(t), v_{d,y}(t), v_{d,z}(t)]^T = \underline{\dot{x}}_d(t) \in \mathbb{R}^3$ is the desired linear velocity vector. In (10), the positive scalars λ_x, λ_y and λ_z are positive design parameters. In the design of the thrust $f_{th}(t)$, we incorporate three terms of the nominal thrust $f_{nom}(t)$, the estimated thrust loss $\hat{f}_{loss}(t)$, as well as $-\alpha|e_v(t)|^{\frac{1}{2}} \operatorname{sign}(e_v(t))$ to study the stability of the cascade system with a "weak" separation principle recovery, as discussed later. To do so, we design an intermediate nominal control $u_{nom}(t) = R(t)[0, 0, f_{nom}(t)]^T = [u_x(t), u_y(t), u_z(t)]^T$ as

$$u_i = -k_{1,i}|\sigma_i(t)|^{\frac{1}{2}} \operatorname{sign}(\sigma_i(t)) + w_i(t) + f_i(t), \tag{11a}$$

$$\dot{w}_i(t) = -k_{2,i} \operatorname{sign}(\sigma_i(t)), \tag{11b}$$

for $i \in \{x, y, z\}$, where $k_{1,i}$ and $k_{2,i}$ are positive design parameters, and

$$f_x(t) = a_{d,x}(t) + \frac{D_x(t)}{M} - \lambda_x\left(v_x(t) - v_{d,x}(t)\right), \tag{12a}$$

$$f_y(t) = a_{d,y}(t) + \frac{D_y(t)}{M} - \lambda_y\left(v_y(t) - v_{d,y}(t)\right), \tag{12b}$$

$$f_z(t) = a_{d,z}(t) + \frac{T_z(t)}{M} - \lambda_z\left(v_z(t) - v_{d,z}(t)\right), \tag{12c}$$

where $T_z(t) = D_z(t) + L_z(t) + Mg$, whilst $\underline{a}_d(t) = [a_{d,x}(t), a_{d,y}(t), a_{d,z}(t)]^T = \underline{\ddot{x}}_d(t) \in \mathbb{R}^3$ is the desired acceleration vector. Now, taking (2) into account, the thrust $f_{th}(t)$ and the desired Euler angle $\underline{\Phi}_d(t) = [\phi_d(t), \theta_d(t), \psi_d(t)]^T$, for a given yaw angle $\psi_d(t)$, are designed as

$$f_{th}(t) = M f_{nom}(t) + \hat{f}_{loss}(t) - \alpha|e_v(t)|^{\frac{1}{2}} \operatorname{sign}(e_v(t)), \tag{13a}$$

$$f_{nom}(t) = \sqrt{u_x^2(t) + u_y^2(t) + u_z^2(t)}, \tag{13b}$$

$$\theta_d(t) = tan^{-1}\left(\frac{C_{\psi_d}(t)u_x(t) + S_{\psi_d}(t)u_y(t)}{u_z(t)}\right), \tag{13c}$$

$$\phi_d(t) = sin^{-1}\left(\frac{S_{\psi_d}(t)u_x(t) - C_{\psi_d}(t)u_y(t)}{f(t)}\right). \tag{13d}$$

The desired angular velocity $\underline{\omega}_d^B(t)$ is designed as

$$\underline{\omega}_d^B(t) = -\lambda_\omega R_q(\underline{\Phi}(t))\left(\underline{\Phi}(t) - \underline{\Phi}_d(t)\right), \tag{14}$$

where λ_ω is a positive design parameter.

Theorem 1. *Consider the dynamics in (1), under Assumption 1. Design the control (13) and (14), with (11) and (12), the sliding surfaces from (10) and the fault estimation from (8). Then, the closed-loop system with estimation error dynamics (9) constructs a cascade system that is FT stable, and then the UAV trajectory $\underline{x}(t)$ converges exponentially to $\underline{x}_d(t)$, for any $\underline{x}(0)$. Also, the control signal is continuous.*

Proof: We rewrite the UAV dynamics (1b) as

$$\dot{\underline{v}}(t) = \frac{R(t)}{M}\begin{bmatrix} 0 \\ 0 \\ f_{th}(t) - f_{loss}(t) \end{bmatrix} - \frac{1}{M}\begin{bmatrix} D_x(t) \\ D_y(t) \\ T_z(t) \end{bmatrix}. \tag{15}$$

Using the designed control (13a), and the fault estimation (8) in (15), it is easy to show that

$$\dot{\underline{v}}(t) = R(t)\begin{bmatrix} 0 \\ 0 \\ f_{nom}(t) \end{bmatrix} + \frac{R(t)}{M}\begin{bmatrix} 0 \\ 0 \\ -\mu(t) \end{bmatrix} - \frac{1}{M}\begin{bmatrix} D_x(t) \\ D_y(t) \\ T_z(t) \end{bmatrix} \tag{16}$$

where $\mu(t)$, defined in Lemma 3, is a continuous function. For the sake of notation, we define $R(t)[0,0,-\mu(t)]^T/M = [\vartheta_x(t), \vartheta_y(t), \vartheta_z(t)]^T$. Therefore, taking into account (11), it is readily obtained that

$$\Pi_{cnt,i} \triangleq \begin{cases} \dot{\sigma}_i(t) = -k_{1,i}|\sigma_i(t)|^{\frac{1}{2}}\,\mathrm{sign}(\sigma_i(t)) + \eta_i(t) \\ \dot{\eta}_i(t) = -k_{2,i}\,\mathrm{sign}(\sigma_i(t)) + \dot{\vartheta}_i(t). \end{cases} \tag{17}$$

for $i \in \{x,y,z\}$. As discussed in Lemma 3, one can see that $|\dot{\mu}(t)| \leq \beta + \bar{f}_1$. Furthermore, $\dot{R}(t) = R(t)[\omega^B(t)]_\times$ which is bounded for bounded variation of rotational speed, guaranteed by (14). Therefore, $\dot{\vartheta}_i(t)$ is bounded, *i.e.*, $\left|\dot{\vartheta}_i(t)\right| \leq \bar{\vartheta}_i$. Therefore, by proper choice of $k_{1,i}$ and $k_{2,i}$ and taking Lemma 1 into account, one can conclude that $\sigma_i(t)$ and $\eta_i(t)$ converge to zero in FT, *i.e.*, a second-order sliding convergence. Since the estimation error $e_v(t)$ contributes to the closed-loop dynamics via $\mu(t)$, (9) and (17) construct a cascade system. Now, we consider the stability of the cascade systems Π_{obs}, defined in (9) and $\Pi_{cnt,i}$, defined in (17), we follow the same approach as in [25, Theorem 5.1], using Lemma 2. It is worth noting that the traditional approach for stability analysis, *e.g.*, [26, Lemma 8], is not applicable here, since the function $f(x) = |x(t)|^{0.5}\,\mathrm{sign}(x(t))$ in (9) and (17) is not Lipschitz. From Lemma 3, we see that $X_{obs}(t) \triangleq [e_v(t), \mu(t)]^T$ converge to zero in FT, *i.e.*, $X_{obs}(t) = 0$ for $t \geq T_o(X_{obs}(0))$. Also, the trajectory $X_{cnt,i}(t) \triangleq [\sigma_i(t), \eta_i(t)]^T$ cannot escape to infinity in FT [24]. Also, $\left|\dot{\vartheta}_i(t)\right| \leq \bar{\vartheta}_i$. On the other hand, as discussed in Lemma 3, $\mu(t)$ is bounded and vanishes in finite time. Therefore, $\int_0^\infty \dot{\vartheta}_i(t)(\tau)d\tau$ is finite. Therefore, according to Lemma 2 and [25, Theorem 5.1], the cascade systems Π_{obs} and $\Pi_{cnt,i}$ make the origin FT stable. On the other hand, $\mu(t) = 0$ for $t \geq T_o(X_{obs}(0))$. Therefore, from (16), one can see that the nominal behavior of the closed-loop dynamics is recovered for $t \geq T_o(X_{obs}(0))$. Then, $\sigma_i(t)$ and $\eta_i(t)$ converge to zero in finite time, $T_c = \max_{i\in\{x,y,z\}} T_{c,i}(X_{cnt,i}(T_o))$, and, considering (10), the UAV trajectory $\underline{x}(t)$ converges exponentially to $\underline{x}_d(t)$, for any initial conditions $\underline{x}(0)$. The stability of the nominal control is straightforward and is therefore omitted. On the other hand, by investigating the control (13a) and (13b) with (11), (12) and (8), it is evident that the commanded control signal is continuous since there is not any discontinuous term contributing in it. □

Corollary 1. *Weak separation principle recovery [25]: The observer gains in (8) can be designed independent of the control ones to achieve the finite time convergence. However, for the control gains in (11), considering the closed-loop dynamics (17), one needs to take the choice of β into account, Even though the FT convergence of the observer and stability of the cascade system, provide a relaxed condition in practice, theoretically, the choice of β affects the choice of $k_{2,i}$. This recovers "almost" a separation principle, hence, it is called the "weak separation principle".*

Remark 3. *In the designed control (13a), it is worth noting the use of the term $\alpha|e_v(t)|^{\frac{1}{2}}\,\mathrm{sign}(e_v(t))$. Without using this term, one can obtain the closed-loop dynamics as*

$$\dot{\underline{v}}(t) = R(t)\begin{bmatrix} 0 \\ 0 \\ f_{nom}(t) \end{bmatrix} + \frac{R(t)}{M}\begin{bmatrix} 0 \\ 0 \\ \dot{e}_v(t) \end{bmatrix} - \frac{1}{M}\begin{bmatrix} D_x(t) \\ D_y(t) \\ T_z(t) \end{bmatrix}.$$

By taking into account (11), defining $R(t)[0,0,\dot{e}_v(t)]^T/M = [e_{v,x}(t), e_{v,y}(t), e_{v,z}(t)]^T$ this further yields

$$\begin{aligned} \dot{\sigma}_i(t) &= -k_{1,i}|\sigma_i(t)|^{\frac{1}{2}}\,\mathrm{sign}(\sigma_i(t)) + \hat{w}_i(t) + e_{v,i}(t), \\ \dot{w}_i(t) &= -k_{2,i}\,\mathrm{sign}(\sigma_i(t)), \end{aligned}$$

for $i \in \{x,y,z\}$, which has a super-twisting structure. However, to use Lemma 1, one needs to satisfy the boundedness of $\dot{e}_{v,i}(t)$, which roots in the boundedness of $\ddot{e}_v(t)$. Considering (9), it is obvious that it is confirmed as $\alpha|e_v(t)|^{\frac{1}{2}}\,\mathrm{sign}(e_v(t))$ is not C^1, while this is avoided in Theorem 1.

Remark 4. *The STC itself can be robust against faults, but with compensation, the convergence to the desired trajectory is faster as verified in the experiments.*

IV. EXPERIMENTAL EVALUATION

As illustrated in Fig.1, we use a customized QAV250 model, equipped with a Pixhwak CUAV V5 Nano autopilot running the PX4 1.12 operating system. We use a Raspberry Pi 4 Model B as the onboard computer, running an Ubuntu server and the noetic version of the Robot Operating System, for communication. The Optitrack system determines the UAV position and orientation externally at a frequency of 120 (Hz). The onboard computer receives the estimated position and orientation over WiFi and relays it to the autopilot. The autopilot uses an extended Kalman filter to fuse these with acceleration and angular rate measurements to estimate the UAV states, and relay it back to the mavros node. It should be noted that the normalized thrust commanded by the default controller of the autopilot is recorded to determine the thrust scaling factor. Then, the total accelerations determined by the STC are normalized using this scaling factor. The STC and STO are implemented at a frequency of 200 (Hz) in a ground laptop running Matlab, which has access to the UAV states from the onboard computer. After commanding the control inputs, the low-level attitude-rate controller in the autopilot determines and commands the PWM motor control inputs. A circular reference trajectory is defined as $\underline{x}_d(t) = [\cos(0.5t), \sin(0.5t), 1.5]^T(m)$. Two types of faults, additive and effectiveness loss, are considered. The effectiveness loss is modeled as $(1-\Delta k(t))f_{th}(t)$, where $\Delta k(t)$ denotes the reduction of the effectiveness. Therefore, the effectiveness loss can be considered as $f_{loss}(t) = \Delta k(t) f_{th}(t)$. The fault

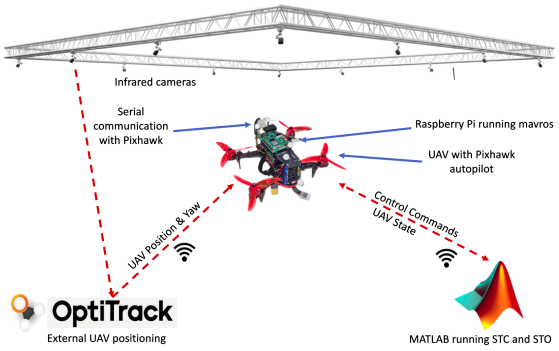

Fig. 1: Illustration of the experimental setup.

is introduced abruptly and gradually, hence, four different experiments are carried out, as shown in the video[1]. The performance is evaluated with and without fault compensation and in the presence and absence of faults. A 60 (s) flight test is divided into four intervals. During 0-15 (s), no fault is introduced while compensation is on. At 15 (s), a fault is introduced and lasts until 45 (s). Fault compensation is turned off at 30 (s) until the end. We choose $\alpha = 1.30$ and $\beta = 0.825$. The lift and drag coefficients in the aerodynamic model are obtained experimentally as $C_L = 1.2$ and $C_D = 0.04$. We choose $\lambda_x = \lambda_y = \lambda_z = 4$, and $\lambda_\omega = 1.0$. Also, $k_{1,i}$ and $k_{2,i}$, for $i \in \{x, y\}$ are chosen based on Remark 1, with $d_1 = 0.1$, and for $k_{1,z}$ and $k_{2,z}$ with $d_1 = 0.05$. For abrupt additive and effectiveness faults, 1.0 (m/s^2) and $\Delta k = 10$ % thrust losses are used, respectively. For gradual additive fault, thrust loss is increased linearly from 0 to 1.0 (m/s^2) in 15 (s) and eliminated at the same rate. For gradual effectiveness faults, the effectiveness is decreased from 100 to 90 %, *i.e.*, $\Delta k = 10\%$, in 15 (s) and then increased to 100 % at the same rate. The fault is injected numerically by reducing the thrust, computed by the STC, just before commanding control.

The tracking errors $\underline{e}(t) = [e_x(t), e_y(t), e_z(t)]^T = \underline{x}(t) - \underline{x}_d(t)$, estimated fault $\hat{f}_{loss}(t)$, and estimated effectiveness loss $\hat{\Delta}k(t) = \hat{f}_{loss}(t)/f_{th}(t)$ are presented in Fig. 2. The Root Mean Square (RMS) errors for each of the fault types and phases of the maneuvers are presented in Table I. It can be seen from Figs. 2 (a) and (b), that the proposed STO accurately estimates the actual thrust loss. Ignoring the first few seconds until the STC starts sliding, the tracking errors converge to within 0.05 (m) until 30 (s) when the compensation is on. There is a momentary increase in tracking error to 0.1 (m) after 15 (s) when the fault is injected abruptly, until the STO reaches sliding again in Fig. 2 (a). However, no such momentary increase in tracking errors is observed when the fault is injected gradually, in Fig. 2 (b). The controller performance is similar to that of one without any fault, hence, the proposed controller recovers the UAV's normal behavior when the fault is injected. When the compensation is turned off at 30 (s), the UAV gradually loses its altitude by around 1.0 (m) in Fig. 2 (a). However, this loss was small and around 0.5 (m) in the gradual additive fault case as the loss was being removed gradually in Fig. 2 (b). In both cases, the UAV overshoots the desired altitude when the fault is completely removed at 45 (s). It can be seen clearly that without STO and compensation, the STC, alone, is not fully effective in handling faults, and takes a long time to recover the UAV properly. It can be seen in Figs. 2 (c) and (d) and Table I, that in the case of effectiveness loss, the tracking results are similar to that of the additive fault. It is worth noting that for effectiveness loss, there can be a residual order of $O(\Delta k^2)$ that affects the closed-loop dynamics. So, the fault effect is partially not compensated.

[1] https://youtu.be/IPZ4OvBH85U

Remark 5. *A quadrotor UAV generates negative lift while flying horizontally due to a negative angle of attack between the plane of propellers and freestream velocity. The lift force is usually not modeled as it is lumped with uncertainty and addressed by the controller. If not modeled, it is captured by the observer and leads to inaccurate fault estimation.*

TABLE I: RMS errors (m) of altitude for different faults.

Duration (s) / **Loss type**	**0-15**	**15-30**	**30-45**	**45-60**
	Compensation on		**Compensation off**	
	Fault off	**Fault on**		**Fault off**
Abrupt additive	0.019	0.032	0.260	0.306
Gradual additive	0.014	0.007	0.220	0.113
Abrupt effectiveness	0.014	0.066	0.278	0.349
Gradual effectiveness	0.008	0.010	0.193	0.105

V. CONCLUSIONS

Accurate trajectory tracking in the presence of thrust loss in a quadrotor unmanned aerial vehicle was addressed in this work, by the design of a super-twisting observer and a super-twisting low-level controller. At the low level, we designed the acceleration commands, and the desired thrust, Euler angles, and angular speeds were computed. We studied the finite-time convergence, the stability of the cascade system, and the recovery of the nominal behavior as well as the weak separation principle. Finally, various experiments were conducted to highlight the effectiveness and performance of the proposed algorithm.

REFERENCES

[1] L. Cui, X. Hou, Z. Zuo, and H. Yang, "An adaptive fast super-twisting disturbance observer-based dual closed-loop attitude control with fixed-time convergence for uav," *J. Franklin Inst.*, vol. 359, no. 6, pp. 2514–2540, 2022.

[2] H. Habibi, D. V. Rao, J. L. Sanchez-Lopez, and H. Voos, "On sora for high-risk uav operations under new eu regulations: Perspectives for automated approach," in *2023 Int. Conf. Unmanned Aircraft Syst. (ICUAS)*, IEEE, 2023, pp. 213–220.

[3] J. A. C. González, O. Salas-Peña, and J. De León-Morales, "Observer-based super twisting design: A comparative study on quadrotor altitude control," *ISA Trans.*, vol. 109, pp. 307–314, 2021.

[4] O. Mofid, S. Mobayen, C. Zhang, and B. Esakki, "Desired tracking of delayed quadrotor uav under model uncertainty and wind disturbance using adaptive super-twisting terminal sliding mode control," *ISA Trans.*, vol. 123, pp. 455–471, 2022.

[5] H. Liu, M. H. C. Man, and K. H. Low, "Uav airborne collision to manned aircraft engine: Damage of fan blades and resultant thrust loss," *Aerosp. Sci. Technol.*, vol. 113, p. 106 645, 2021.

[6] G. K. Fourlas and G. C. Karras, "A survey on fault diagnosis and fault-tolerant control methods for unmanned aerial vehicles," *Machines*, vol. 9, no. 9, p. 197, 2021.

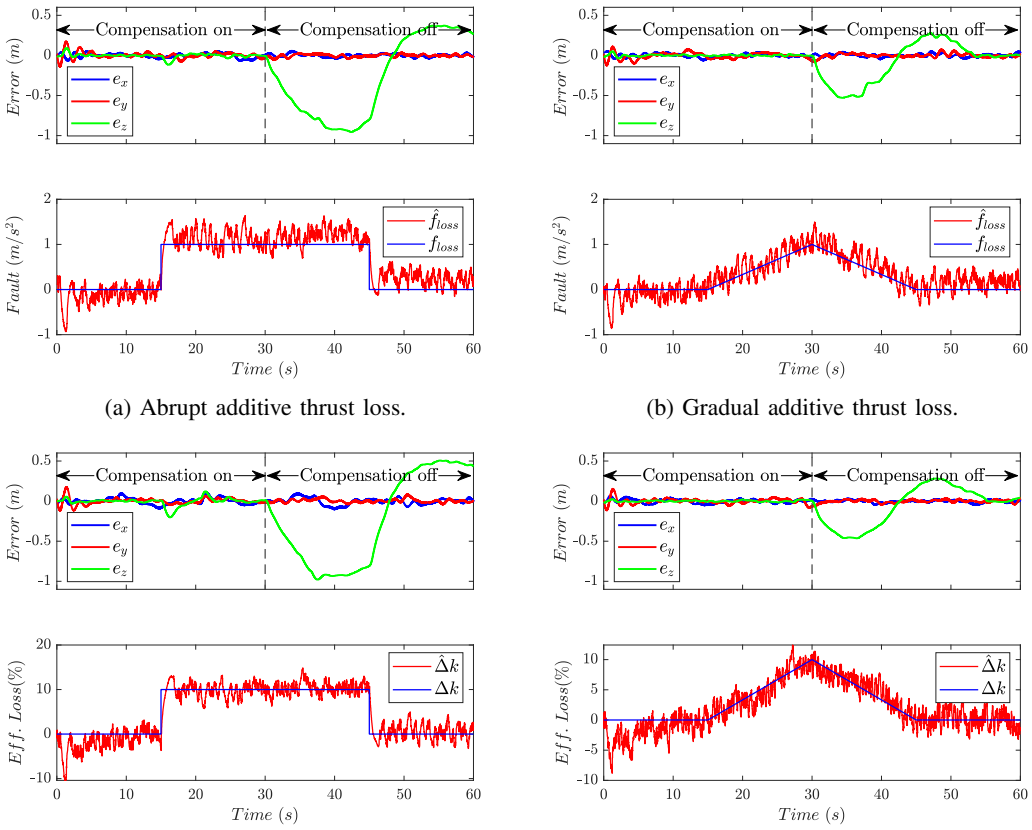

(a) Abrupt additive thrust loss.

(b) Gradual additive thrust loss.

(c) Abrupt effectiveness loss.

(d) Gradual effectiveness loss.

Fig. 2: Time histories of tracking errors and estimated fault and effectiveness.

[7] S. Mallavalli and A. Fekih, "A fault tolerant control design for actuator fault mitigation in quadrotor uavs," in *2019 American Control Conf. (ACC)*, IEEE, 2019, pp. 5111–5116.

[8] D. Ma, Y. Xia, G. Shen, Z. Jia, and T. Li, "Flatness-based adaptive sliding mode tracking control for a quadrotor with disturbances," *J. Franklin Inst.*, vol. 355, no. 14, pp. 6300–6322, 2018.

[9] M. Labbadi and M. Cherkaoui, "Robust adaptive backstepping fast terminal sliding mode controller for uncertain quadrotor uav," *Aerosp. Sci. Technol.*, vol. 93, p. 105 306, 2019.

[10] J.-J. Xiong and G.-B. Zhang, "Global fast dynamic terminal sliding mode control for a quadrotor uav," *ISA Trans.*, vol. 66, pp. 233–240, 2017.

[11] O. Mofid and S. Mobayen, "Adaptive finite-time backstepping global sliding mode tracker of quad-rotor uavs under model uncertainty, wind perturbation, and input saturation," *IEEE Trans. Aerosp. Electron. Syst.*, vol. 58, no. 1, pp. 140–151, 2021.

[12] A. Raza, F. M. Malik, N. Mazhar, H. Ullah, and R. Khan, "Finite-time trajectory tracking control of output-constrained uncertain quadrotor," *IEEE Access*, vol. 8, pp. 215 603–215 612, 2020.

[13] O. Mofid and S. Mobayen, "Adaptive sliding mode control for finite-time stability of quad-rotor uavs with parametric uncertainties," *ISA Trans.*, vol. 72, pp. 1–14, 2018.

[14] L. Besnard, Y. B. Shtessel, and B. Landrum, "Quadrotor vehicle control via sliding mode controller driven by sliding mode disturbance observer," *J. Franklin Inst.*, vol. 349, no. 2, pp. 658–684, 2012.

[15] R. Jiao, W. Chou, Y. Rong, and M. Dong, "Anti-disturbance control for quadrotor uav manipulator attitude system based on fuzzy adaptive saturation super-twisting sliding mode observer," *Appl. Sci.*, vol. 10, no. 11, p. 3719, 2020.

[16] L. Cui, R. Zhang, H. Yang, and Z. Zuo, "Adaptive super-twisting trajectory tracking control for an unmanned aerial vehicle under gust winds," *Aerosp. Sci. Technol.*, vol. 115, p. 106 833, 2021.

[17] H. Ríos, R. Falcón, O. A. González, and A. Dzul, "Continuous sliding-mode control strategies for quadrotor robust tracking: Real-time application," *IEEE Trans. Indust. Elect.*, vol. 66, no. 2, pp. 1264–1272, 2018.

[18] J. L. Sanchez-Lopez, M. Castillo-Lopez, M. A. Olivares-Mendez, and H. Voos, "Trajectory tracking for aerial robots: An optimization-based planning and control approach," *J. Intell. Robot. Syst.*, vol. 100, no. 2, pp. 531–574, 2020.

[19] H. Zhu and J. Alonso-Mora, "Chance-constrained collision avoidance for mavs in dynamic environments," *IEEE Robot. Autom. Lett*, vol. 4, no. 2, pp. 776–783, 2019.

[20] J. L. Sanchez-Lopez, M. Wang, M. A. Olivares-Mendez, M. Molina, and H. Voos, "A real-time 3d path planning solution for collision-free navigation of multirotor aerial robots in dynamic environments," *J. Intell. Robot. Syst.*, vol. 93, no. 1, pp. 33–53, 2019.

[21] H. Habibi, A. Safaei, H. Voos, M. Darouach, and J. L. Sanchez-Lopez, "Safe navigation of a quadrotor uav with uncertain dynamics and guaranteed collision avoidance using barrier lyapunov function," *Aerosp. Sci. Technol.*, p. 108 064, 2023.

[22] A. Safaei and M. N. Mahyuddin, "Optimal model-free control for a generic mimo nonlinear system with application to autonomous mobile robots," *Int. J. Adapt. Control Signal Process.*, vol. 32, no. 6, pp. 792–815, 2018.

[23] J. A. Moreno and M. Osorio, "Strict lyapunov functions for the super-twisting algorithm," *IEEE Trans. Automatic Control*, vol. 57, no. 4, pp. 1035–1040, 2012.

[24] A. Chalanga, S. Kamal, L. M. Fridman, B. Bandyopadhyay, and J. A. Moreno, "Implementation of super-twisting control: Super-twisting and higher order sliding-mode observer-based approaches," *IEEE Trans. Indust. Elect.*, vol. 63, no. 6, pp. 3677–3685, 2016.

[25] J. A. Moreno, "A lyapunov approach to output feedback control using second-order sliding modes," *IMA J. Math. Control. Inf.*, vol. 29, no. 3, pp. 291–308, 2012.

[26] H. Habibi, A. Yazdani, M. Darouach, H. Wang, T. Fernando, and I. Howard, "Observer-based sensor fault tolerant control with prescribed tracking performance for a class of nonlinear systems," *IEEE Trans. Auto. Control*, vol. 68, no. 12, pp. 8259–8266, 2023.